Properties of ridges in elastic membranes

Alexander E. Lobkovsky* and T. A. Witten
The James Franck Institute, The University of Chicago, 5640 South Ellis Avenue, Chicago, Illinois 60637
(Received 19 August 1996)

When a thin elastic sheet is confined to a region much smaller than its size the morphology of the resulting crumpled membrane is a network of straight ridges or folds that meet at sharp vertices. A virial theorem predicts the ratio of the total bending and stretching energies of a ridge. Small strains and curvatures persist far away from the ridge. We discuss several kinds of perturbations that distinguish a ridge in a crumpled sheet from an isolated ridge studied earlier [A. E. Lobkovsky, Phys. Rev. E **53**, 3750 (1996)]. Linear response as well as buckling properties are investigated. We find that, quite generally, the energy of a ridge can change by no more than a finite fraction before it buckles. [S1063-651X(97)02002-3]

PACS number(s): 03.40.Dz, 46.30.−i, 68.55.Jk

I. INTRODUCTION

There is an abundance of phenomena involving strong deformation of thin elastic membranes that span a wide range of scales. On the microscopic scale, phospholipid membranes behave like a solid below a two-dimensional (2D) freezing point [1]. Some inorganic compounds such as graphite oxide [2] and molybdenum disulphite [3] also behave like elastic membranes on scales large compared to the interatomic spacing. The graphite oxide sheets can be collapsed in solution by inducing an effective attractive interaction between distant parts of the sheet. Molybdenum disulphite has also been observed in a ''rag'' phase that looks similar to a crumpled piece of paper. Mechanical properties of macroscopic thin elastic plates and shells undergoing large deformations are important in engineering of safety structures [4] and packaging material development [5].

Stability and post-bucking properties of thin shells and plates have been a subject of intense investigation [6]. Few general results have been derived, however. Due to the complexity of the equations that describe large deflections of thin plates (two quadratic fourth-order partial differential equations), rigorous proofs are difficult to achieve. Difficulties in treating thin shells and plates arise due to the fact that a small parameter related to the thickness of the shell multiplies the highest derivative term in the equations [7]. It is well known that this fact gives rise to a variety of boundary layer phenomena in the bending of thin shells [8]. Many different types of boundary conditions that lead to a boundary layer have been analyzed. They include bending moments [9], shear forces [10], and free boundary conditions with distributed bending moments [11]. A common feature that emerges from these studies is that membrane stresses become confined to the boundary layer region whose size vanishes as some power of the shell thickness.

The study of the buckling instability and post-buckling behavior of thin plates and shells is a well-developed field within the discipline of continuum mechanics. For a review of the methods and results see, for example, Ref. [12]. Buckling instability is always treated perturbatively. This level of analysis is sufficient for determining the buckling pattern as a function of the loading. Discussions of the post-buckling behavior are highly problem specific, however. The authors of Ref. [13], for example, realized that in the limit of the vanishing thickness, the diamond buckling pattern of a cylindrical shell consists of almost flat facets and almost sharp ridges. Understanding of the mechanism that governs the sharpness of the ridges and their energy is lacking, however. A similar phenomenon was observed in strong axisymmetric buckling of a spherical shell by Scheidl and Troger [14]. The sharp circular ridge was identified as the boundary layer that joins the solutions in the two weakly deformed regions of the shell. The boundary layer width was found to scale with the square root the shell thickness.

It has been suggested recently by the author and others [15,16] that membrane stresses in a strongly crumpled elastic sheet are confined to a set of straight ridge singularities or folds. These ridge singularities, which were shown to arise under quite general conditions, constitute another case of the boundary layer phenomena in thin plates. A scaling law for the ridge width as a function of the plate thickness had been established with the use of an energy scaling argument [15] and a boundary layer analysis of von Kármán thin plate equations [16]. Elastic energy was found to be confined in the ridges and to scale as 1/3 power of the size of the ridge for a fixed plate thickness. Other scaling laws such as the dependence of the ridge width and energy on the dihedral angle were also investigated.

In this article we extend the analytical and numerical study of the ridges to explore whether the results obtained for isolated ridges can be successfully applied to a network of interacting ridges in a crumpled elastic sheet. In Sec. II we introduce the concept of the ''minimal ridge,'' which refers to the necessary and sufficient conditions leading to the formation of the ridge singularity in the limit of the vanishing plate thickness. Deviations from these ''minimal'' boundary conditions in a crumpled sheet can then be treated, at least in the first approximation, as perturbations to the minimal ridge. In Sec. III we discuss a ''virial theorem'' for ridges that is a direct consequence of the energy scaling argument. It provides a useful tool in testing the confinement of elastic energy and the degree to which ridge interaction influences

*Electronic address: a-lobkovsky@uchicago.edu; World Wide Web homepage: http://rainbow.uchicago.edu/~lobkovsk

it. In Sec. IV we present a scaling argument and an extension of the asymptotic analysis of the von Kármán equations that establish that there is a long-range decay of the longitudinal ridge curvature and the transverse stress far away from the ridge. The energy in these ridge ''echoes'' is negligible compared to the energy of the ridge. A perturbation framework for dealing with external forcing of the minimal ridge is presented in Sec. V. A particular case of the ridge compression is studied in detail and the scaling of the elastic energy correction is found. We show in Sec. VI that the small echo strains and curvatures are sufficient to change the energy of a far away ridge by a finite fraction. Numeric evidence corroborating some of the claims made in the previous sections is presented in Sec. VII. Finally, implications of the ridge properties for the crumpling problem as well as future work are discussed in Sec. VIII.

II. THE ''MINIMAL'' RIDGE

To facilitate a study of the ridge singularity one must first write down equations that describe large deflections of thin plates. Second, an understanding of the conditions that lead to the formation of the ridge singularity must be achieved. It was suggested in Ref. [16] that the existence of the sharp vertices where both radii of curvature are of the order of the sheet thickness is a necessary and sufficient condition for the formation of ridges. Ridges connect these points of high curvature. A minimal way to create a ridge, therefore, Ref. [16] argued, is to introduce sharp points at the boundary of a flat rectangular piece of elastic material by requiring that its boundary follow a frame that has a sharp bend. The von Kármán equations that describe large deflections of thin elastic plates can be used to deduce the asymptotic behavior of the ridge solution in this simple geometry.

Let us recall the boundary-value problem that exhibits the ridge singularity [16]. Consider a strip made of isotropic homogeneous elastic material with Young's modulus Y and Poisson ratio ν. It has thickness h and width X. The points are labeled by the material coordinates (x,y) so that $x \in (-X/2,X/2)$. The strip extends in the y direction. Normal forces are applied to the long boundaries $x=\pm X/2$ in such a way as to force the boundary to follow a rectilinear frame that has a sharp bend at $y=0$. The bend dihedral angle is $\pi-2\alpha$ (so that $\alpha=0$ corresponds to a flat strip). The shape of the strip and the elastic stresses are found from a solution to the nondimensionalized von Kármán equations

$$\nabla^4 f=[\chi,f], \tag{1a}$$

$$\lambda^2\nabla^4\chi=-\frac{1}{2}[f,f]. \tag{1b}$$

Here $\nabla^4\equiv\nabla^2\nabla^2$ and a set of square brackets $[a,b]$ denotes a symmetric contraction of the second derivatives of the fields a and b,

$$[a,b]\equiv\epsilon_{\alpha\mu}\epsilon_{\beta\nu}(\partial_\alpha\partial_\beta a)(\partial_\mu\partial_\nu b) =\frac{\partial^2 a}{\partial x^2}\frac{\partial^2 b}{\partial y^2}+\frac{\partial^2 a}{\partial y^2}\frac{\partial^2 b}{\partial x^2}-2\frac{\partial^2 a}{\partial x\partial y}\frac{\partial^2 b}{\partial x\partial y}. \tag{2}$$

Here $\epsilon_{\alpha\beta}$ is the antisymmetric 2×2 tensor. Summation over repeated indices is implied.

All lengths are measured in terms of the strip width X and energies in terms of the bending rigidity $\kappa=Yh^3/12(1-\nu^2)$. The first von Kármán equation is the statement of the local normal force equilibrium. The second one has a purely geometric origin. It simply states that Gaussian curvature $-\frac{1}{2}[f,f]$ acts as a source for the stress field. The small parameter $\lambda\sim h/X$ is proportional to the dimensionless thickness of the sheet. Here $f(x,y)$ and $\chi(x,y)$ are the potentials whose derivatives give the curvatures $C_{\alpha\beta}$ and the two dimensional in-plane stresses $\sigma_{\alpha\beta}$ via

$$C_{\alpha\beta}=X^{-2}\partial_\alpha\partial_\beta f, \tag{3}$$

$$\sigma_{\alpha\beta}=\kappa X^{-2}\epsilon_{\alpha\mu}\epsilon_{\beta\nu}\partial_\mu\partial_\nu\chi. \tag{4}$$

To clarify the meaning of the curvature tensor $C_{\alpha\beta}$ we note that its eigenvalues are the inverses of the principal radii of curvature of the sheet. The sheets assumes a conformation that minimizes the elastic energy consisting of the bending and the stretching parts (measured in the units of κ)

$$E_{\text{bend}}=\int dx\,dy[\nabla^2 f]^2, \tag{5a}$$

$$E_{\text{str}}=\lambda^2\int dx\,dy[\nabla^2\chi]^2. \tag{5b}$$

There are two ways to supply boundary conditions for the von Kármán plate equations consistently. First, one could specify a Kirchoff-type condition on the functions f and χ and their derivatives in terms of the *material* coordinates. Second, a prescribed shape in the *embedding* space corresponds to clamping the boundaries of the strip or simply supporting them. Only the first type of boundary condition is tractable in general since the relation between the derivatives of the functions f and χ and the shape of the sheet in the embedding space is nonlinear. In addition, even if one succeeds in translating the boundary conditions that make reference to the embedding space into the language of f and χ, they will *change* when the thickness of the sheet is varied or external forces are applied. Therefore, only when the stresses and curvatures are *specified* at the boundary can one make any analytical progress. We must remark at this point that the effective boundary conditions for a ridge in a crumpled sheet are not of this type. Stresses in the facets are nonzero. More importantly, they depend on how each ridge is stressed by the rest of the sheet.

The minimal ridge boundary conditions are given in terms of the curvature at the boundary. The only requirement is that there be two sharp points on each long boundary of the strip. The stresses and torques vanish at the boundary $x=\pm X/2$ (except at the singular point $y=0$)

$$\partial_\alpha\partial_\beta\chi=\partial_\alpha\partial_\beta f=0. \tag{6}$$

The sharp vertices introduced at the boundary can be mathematically expressed as singularity in the curvature at the boundary points $y=0$ and $x=\pm X/2$,

$$\frac{\partial^2 f}{\partial y^2} = \alpha \delta(y). \tag{7}$$

The coefficient α in Eq. (7) is exactly the bending angle α of the frame which is equal to the half of the difference of the dihedral angle of the frame from π [16].

The motivation behind seeking the minimal ridge is that a number of the asymptotic properties of the ridge singularity are independent of the details of the boundary conditions. These include the exponents in the asymptotic thickness scaling of the ridge curvature, elastic energy, and other quantities. Dihedral angle scaling exponents are also independent of the details of the boundary conditions [16]. Other ridge properties, which do depend on the details of the boundary conditions (the longitudinal stress supported by a ridge, for example), can then be found perturbatively, at least in the first approximation. The following two sections explore additional boundary-condition-independent asymptotic properties of the minimal ridge that are useful in the investigation of the effects of the crumpled sheet environment on the minimal ridge.

III. VIRIAL THEOREM

A study of the minimal ridge [16] revealed that as the thickness of the sheet vanished, the shape developed a sharp crease. Details of how that singular limit is approached were found. In particular, the elastic energy concentrates in a small region around the ridge of the size given by the characteristic ridge curvature C. This fact allows one to construct an energy scaling argument that yields the asymptotic scaling behavior of the ridge curvature C and the elastic energy E [17].

For the purpose of the energy scaling argument given in Ref. [17], let us rewrite the expressions for the bending and the stretching energies Eqs. (5) in terms of the principal strains γ_1 and γ_2 and the principal radii of curvature $R_1 \equiv 1/C_1$ and $R_2 \equiv 1/C_2$. We get [18]

$$E_{\text{bend}} = \frac{1}{2}\int dS[\kappa(C_1+C_2)^2 + \kappa_G C_1 C_2], \tag{8a}$$

$$E_{\text{str}} = \frac{1}{2}\int dS[G(\gamma_1+\gamma_2)^2 + G_s \gamma_1 \gamma_2]. \tag{8b}$$

$G = Yh$ is the two-dimensional stretching modulus of a sheet of thickness h made of elastic material with Young's modulus Y. For the purposes of an energy scaling argument we may ignore the second terms in the expressions for the energies. The argument given by Witten and Li in Ref. [17] estimates these energies in terms of a characteristic curvature C, for example, the transverse curvature in the middle of the ridge. According to that argument, if the length of the ridge, i.e., the distance between the vertices, is X, then the characteristic strain $\gamma \sim (CX)^{-2}$ exists in the ridge region of width C^{-1} so that the total stretching energy in the ridge is approximately $E_{\text{str}} \sim G\gamma^2(X/C) \sim GX^{-3}C^{-5}$. Similarly, the bending energy is given by the characteristic ridge curvature C, via $E_{\text{bend}} \sim \kappa C^2(X/C) \sim \kappa XC$. Reference [17] then argued that C is the only parameter that characterizes the ridge. Also, since the bending and the stretching energies both vary as a power of C, they must be comparable when the total energy is minimized. It immediately followed that $C \sim (\kappa/G)^{-1/3}X^{-2/3} \sim h^{-1/3}X^{-2/3}$.

Another important conclusion of the energy scaling argument emerges when we consider the derivative of the energy with respect to the parameter C. It must vanish for the value of C at which the minimum total energy is achieved. Since the energies depend on powers of C we obtain the statement

$$\frac{dE}{dC} = \frac{dE_{\text{str}}}{dC} + \frac{dE_{\text{bend}}}{dC} = \frac{-5E_{\text{str}} + E_{\text{bend}}}{C} = 0, \tag{9}$$

which leads to a ''virial theorem'' for ridges $E_{\text{bend}} = 5E_{\text{str}}$ analogous to the virial theorem relating kinetic to potential energy in celestial mechanics [19]. The validity of this virial theorem rests on rather general grounds. The only requirements are that (a) the energy be rigorously expressible a sum of a bending and a stretching contributions and (b) each of these varies as a *power* of a free parameter, here C. Thus a failure of the virial theorem would indicate that the energies did not vary with the anticipated powers of C. Such a failure would be expected if C^{-1} were comparable to other lengths in the problem, such as the size of the sheet X.

We have performed a numerical test of the virial theorem using a lattice model of an elastic sheet after Seung and Nelson [20]. A numerical verification of the virial theorem for the tetrahedral shape is presented in Sec. VI; here we only remark that the agreement is better than few percent. We must point out that whereas the virial theorem holds in the limit of the vanishing shell thickness, the numerics showed that the ratio of the total bending and stretching energies is predicted by the virial theorem with a 10% accuracy for ridges of the size to thickness ratio greater than 1000. If a view of the crumpled membrane as a network of ridges that meet at vertices is correct, the tetrahedron virial theorem suggests that ridges in a crumpled sheet are well-defined objects to which a scaling argument can be applied.

IV. LARGE-DISTANCE BEHAVIOR OF THE RIDGE SOLUTION

To ascertain how much ridges influence one another in a crumpled sheet one must determine how the boundary-layer solution, which is valid in progressively narrow region around the ridge midline, joins onto the flat solution far away from the ridge. The following development is motivated by an observation that in a numerical implementation of a ridge, the echo strains and curvatures persist far away from the ridge, despite the fact that most of the energy is concentrated into a region of asymptotically vanishing width. In fact, the characteristic decay length L of the echo strains and curvatures may diverge in the $\lambda \to 0$ limit. In this section we present an energy scaling argument for the existence and asymptotic scaling of the decay length L for the minimal ridge configuration. This conclusion is put on a more rigorous footing by an extension of the asymptotic analysis of the von Kármán equations that includes the matching condition between the boundary layer and the large-distance solution. The scaling of the long-distance solution is later supported by numerical evidence.

We imagine cutting the ridge along its midline into two

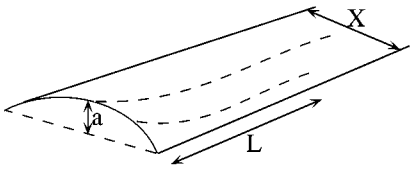

FIG. 1. Gentle curvature at the short end of a semi-infinite strip decays at a characteristic distance L.

identical parts. For the boundary-value problem defined on one of resulting semi-infinite strips, the ridge effectively introduces some complicated boundary conditions applied at the cut. The detailed form of these boundary conditions is not important for our purposes. It is significant, however, that they have no singularities. For the purposes of an energy scaling argument, we imagine that the short side of the semi-infinite strip is slightly bent so that its middle is displaced in the normal direction by an amount a as shown on Fig. 1.

This curvature decays to zero at a characteristic distance L from the short end of the strip. This length is set by the competition of the bending energy that favors quick decay of the curvature and the stretching energy that is smallest when the decay length is large. The bending energy is given by the integral of the squared mean curvature over the area of the strip. If the decay length L is much larger than the vertical displacement a, the dominant curvature is in the x (short) direction and is approximately $C_{xx}\sim a/X^2$. The bending energy is then $E_{\rm bend}\sim\kappa C_{xx}^2 XL\sim\kappa a^2 X^{-3}L$. Here κ is the bending rigidity and XL is the area of the strip where the deformation exists. The strain created by the decay of the transverse curvature C_{xx} is due to the fact that the middle of the sheet is inclined by a small angle of order a/L and thus the projected length of the line that bisects the strip is shorter than the length of the same segment of the boundary. The length mismatch creates a characteristic strain in the y (long) direction $\gamma_{yy}\sim a^2/L^2$. Thus the stretching energy is $E_{\rm str}\sim G\gamma_{yy}^2 XL\sim\kappa h^{-2}a^4 XL^{-3}$. Here we used the fact that the 2D stretching modulus G is related to the bending rigidity via $G\sim\kappa/h^2$. Since both kinds of energies vary as a power of L, they must be comparable when the total energy $E_{\rm bend}+E_{\rm str}$ is minimized. We thus obtain the scaling of the decay length $L\sim X(a/h)^{1/2}$. The displacement a is determined by the scaling properties of the ridge. The asymptotic scaling of $C_{xx}\sim a/X^2$ must be consistent with that of the longitudinal ridge curvature $\partial^2 f/\partial x^2\sim\lambda^{1/3}/X$. Therefore $a\sim X\lambda^{1/3}$, which yields the scaling for the decay length L and the elastic energy in the ridge ''wing'' in the $\lambda\to 0$ limit

$$L\sim X\lambda^{-1/3},\quad E_{\rm wing}\sim\kappa\lambda^{1/3}. \tag{10}$$

Notice that the energy in these ridge wings or echoes is negligible compared to the ridge energy that scales as $\kappa\lambda^{-1/3}$ [15]. This energy is spread over an increasingly large area.

The scaling of the ridge wings can be also obtained from an extension of the asymptotic analysis of the von Kármán equations. Reference [16] determined the scaling of the boundary-layer solution by rescaling all variables by a power of λ as in Eq. (16) and then requiring that the highest derivative terms in Eqs. (1) be of the same order in λ. The exponents of the λ factors that rescaled f and y were identical due to the imposed boundary condition $f=\alpha|y|$ [this a particular way to satisfy Eq. (7)]. Here we are seeking the scaling of the large-distance solution that is pieced together with the ridge solution. Hence we can find such a solution separately for either side of the ridge. This allows for arbitrary rescaling factors for f and y since the large distance behavior of f in the case of the wing is no longer required to be linear in y. The matching condition on, say, $\partial^2 f/\partial x^2$ for some fixed y and $\lambda\to 0$ requires that the wing solution for f scale with λ in the same way as the ridge solution, i.e., $f=\lambda^{1/3}\tilde{f}$, where $\tilde{f}$ is finite in the $\lambda\to 0$ limit. The same reasoning applies to the asymptotic scaling of χ. Thus the rescaling transformation that is needed to determine the scaling of y in the wing solution is

$$f=\lambda^{1/3}\tilde{f},\quad \chi=\lambda^{-2/3}\tilde{\chi},\quad y=\lambda^{\beta}\tilde{y},\quad x=\lambda^{0}\tilde{x}. \tag{11}$$

The longitudinal direction x is not affected by the rescaling transformation and the exponent β must be negative since a positive β would reproduce the boundary layer scaling. Plugging the scaling ansatz Eq. (11) into the von Kármán Eqs. (1) we obtain

$$\lambda^{1/3}\left[\frac{\partial^4\tilde{f}}{\partial\tilde{x}^4}+2\lambda^{-2\beta}\frac{\partial^4\tilde{f}}{\partial\tilde{x}^2\partial\tilde{y}^2}+\lambda^{-4\beta}\frac{\partial^4\tilde{f}}{\partial\tilde{y}^4}\right]=\lambda^{-2/3+1/3-2\beta}[\tilde{\chi},\tilde{f}], \tag{12a}$$

$$\lambda^{2-2/3}\left[\frac{\partial^4\tilde{\chi}}{\partial\tilde{x}^4}+2\lambda^{-2\beta}\frac{\partial^4\tilde{\chi}}{\partial\tilde{x}^2\partial\tilde{y}^2}+\lambda^{-4\beta}\frac{\partial^4\tilde{\chi}}{\partial\tilde{y}^4}\right]=-\frac{1}{2}\lambda^{2/3-2\beta}[\tilde{f},\tilde{f}]. \tag{12b}$$

Balancing the dominant terms we obtain $\beta=-1/3$ in contrast to $\beta=1/3$ for the boundary-layer solution [16]. Therefore, the decay length L of the wing strains and curvatures scales as $X\lambda^{-1/3}$, in agreement with the prediction of the energy scaling argument above. The leading-order behavior of the elastic energy in the wings can be found by substituting the rescaled variables into Eqs. (5). We obtain $E_{\rm wing}\sim\kappa\lambda^{1/3}$ in accord with the energy scaling argument. In Sec. VI we numerically verify the existence of the long-range decay of the curvatures and stresses away from the ridge. The decay length is found to scale as predicted in the small-thickness limit.

V. RIDGE UNDER EXTERNAL FORCING

To assess the relevancy of the results obtained for the minimal ridge to ridges in a crumpled membrane, we must first discuss ways in which the effective boundary conditions for a ridge in a crumpled sheet differ from that of the minimal ridge, and second, we ought to determine how these differences affect such relevant ridge properties as the coefficients in the thickness scaling laws. The additions and changes to the rectilinear frame boundary conditions for the minimal ridge, which distinguish them from realistic boundary conditions for a ridge in a crumpled sheet, can consist of (a) stresses applied at the boundary, (b) torques applied at the boundary, and (c) distributed normal forces that arise when

distant parts of the crumpled sheet press on the ridge.

In this section we discuss the linear response of the minimal ridge to external perturbations. *A priori*, there is no reason to believe that the asymptotic scaling of the linear-response moduli is independent of the details of the boundary conditions that create and, more importantly, maintain the ridge in the process of external loading. In other words, if we have chosen to maintain constant normal forces on the boundaries instead of maintaining constant curvature, the scaling of the linear-response moduli with the thickness could be different. In fact, numerical evidence suggests that the scaling of the ridge stiffness with respect to compression does indeed depend on the way boundary conditions are maintained as the ridge is being distorted. One must therefore address the applicability of the results derived in this section to the determination of the elastic response of crumpled sheets where the details of the boundary conditions are not known. We are unable to address this question here beyond suggesting that the linear response of a regular tetrahedron considered in Sec. VII might reflect the situation in the crumpled sheet given our view of the crumpled membrane as a collection of vertices, ridges, and facets.

A. Linear response to specified boundary forces

We present a treatment that allows one to construct a consistent perturbation expansion in the small external forces that act at the boundary. The case of the distributed external forces can be treated in a similar manner that will be discussed below. This method of treating perturbations is by no means unique. It allows one, however, easily to establish asymptotic scaling of the energy correction in the limit of the vanishing membrane thickness. The essential idea is to reformulate the problem in terms of some new functions f_i and χ_i that are subject to the *unchanged* minimal ridge boundary conditions B_0 but satisfy modified equations. Consider the case when the full boundary forces B_{ext} (including the applied external forces) can be decomposed into $B_{\text{ext}}=B_0+\delta B$. Let f_e and χ_e be the solution to the boundary-value problem δB that includes *only* the small additional forces (i.e., the strip is not bent). We then seek the solution to Eqs. (1) subject to the full boundary conditions in the form

$$f=f_i+f_e, \quad \chi=\chi_i+\chi_e, \tag{13}$$

so that f_i and χ_i are subject to the same boundary conditions B_0 as the undisturbed ridge solution, but satisfy modified equations

$$\nabla^4 f_i=[\chi_i,f_i]+[\chi_e,f_i]+[\chi_i,f_e], \tag{14a}$$

$$\lambda^2\nabla^4\chi_i=-\frac{1}{2}[f_i,f_i]-[f_e,f_i]. \tag{14b}$$

For a sufficiently small perturbation one can construct a series expansion around the unperturbed solution.

The equations for the first-order corrections to the ridge solution are linear and inhomogeneous. The coefficients as well as the source terms are proportional to the second derivatives of the unperturbed minimal ridge solution. These second derivatives are proportional to the stresses and curvatures in the unperturbed ridge. According to Ref. [16], the dominant (dimensionless) stresses and curvatures are of order $\lambda^{-1/3}$ in the region of the ridge of width $\lambda^{1/3}$. Section IV of this article determines the behavior of the stresses and curvatures in the rest of the sheet. The dominant nondimensional stresses and curvatures in the ridge wings are of order $\lambda^{1/3}$. These echo disturbances are spread over a large region of size $L\sim\lambda^{-1/3}$ so that the elastic energy in the wings is negligible compared to the ridge energy. The correction to the ridge solution will possess the same qualitative features as the source terms in Eqs. (14) that determine them. Since the behavior of the source terms in Eqs. (14) is completely determined by the minimal ridge solution we postulate that the perturbing energy is confined to the region of the ridge of width $\lambda^{1/3}$. We will use this feature later to determine the appropriate integration domain for the ridge energy correction due to the external forces.

At this point we must mention how distributed forces could be included in this treatment. On the one hand, we could find the effect of the external forces on the flat strip with free boundaries and then proceed with the derivation as above. On the other hand, distributed normal forces can be directly added to the first von Kármán equation (14a) since it states the normal force balance on an infinitesimal element of the sheet $dxdy$. External in-plane forces lead to a redefinition of the Airy stress function χ. It may not be at all possible to define a stress function when in-plane external forces are present, however. External distributed torques result in a redefinition of f if its definition is indeed possible. This is certainly the case for small deflections when Monge coordinates can be used [16].

The method presented above of splitting the boundary-value problem into two is applicable when several conditions are satisfied. First, note that if the equations were linear, the result of such splitting would be trivial since the equations for f_i and χ_i would be the same as the original equations and the result of the splitting the problem into two amounts to the principle of superposition. Second, the perturbed boundary conditions B_{ext} that include the external force must be *compatible* with the boundary conditions B_0. For compatibility we require that both sets of boundary conditions are supplied in terms of the same functions (and derivatives) of f and χ at the boundary. Thus the change from B_0 to B_{ext} amounts to a change in the boundary *values* of the specified functions. We denote the change in these boundary values schematically as $\delta B\equiv B_{\text{ext}}-B_0$. This condition ensures that the boundary-value problem δB for f_e and χ_e is well posed. Third, we assumed that the part of the boundary conditions B_0 that create the ridge is unchanged in the process of loading.

It is unknown to us whether these conditions are satisfied in a crumpled sheet. We will see below that the prediction based on this method, for the linear response to point forces acting at the vertices of a regular tetrahedron, is incorrect. A possible explanation is that precisely the condition for B_0 to be held constant in the process of loading is violated in the tetrahedron. The effective boundary conditions for each ridge in a tetrahedron, the stresses in the facets, for example, may change in proportion to the forces acting at the vertices. However, it might be possible to modify the conclusions of this method for a general case of changing boundary conditions. Certain features that emerge from the perturbation

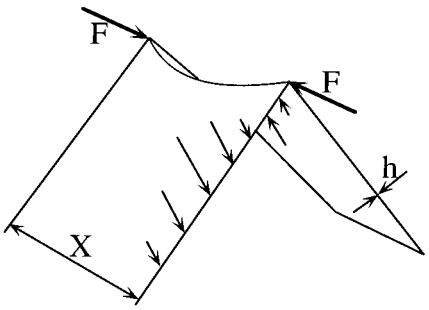

FIG. 2. Long strip of width X, bent by normal boundary forces (one-quarter of which are shown) and compressed by forces F applied at the vertices.

scheme are likely to survive for a general loading. In particular, the effect of the perturbation is likely to be confined to the ridge region as above.

Another limitation of this method stems from the arbitrariness of the choice of the external load. In other words, of all possible ways to load the ridge, the one in the ridge's ''weakest direction'' is relevant to determination of the elastic response of crumpled sheets. It may happen that due to high symmetry, the chosen load does not ''have a component in the weakest direction'' of the ridge. As a result, the stiffness of the ridge in response to such a load is qualitatively greater than its stiffness with respect to a generic load. The concepts in quotes above can be made rigorous. We discuss various types of loading in Sec. V D with regard to their relevance to the determination of the weakest ridge modulus.

B. Point forces applied at the ridge vertices

The analysis can be carried further when the external influence is characterized by a single small dimensionless parameter $\overline{F}$. In particular, for most of the following development, we explicitly consider the case of compression of the ridge by a pair of point forces acting at the ridge vertices as shown on Fig. 2. Presumably, there are loads for which the asymptotic λ scaling of the solution to the ''flat'' problem f_e and χ_e is different from that in the case of the point forces. This, however, introduces but a few changes in the following derivation.

A flat strip compressed by a pair of point forces acting at the boundary remains flat for small enough forces. In addition, the stress function is linear in the applied force $\overline{F}$,

$$f_e(x,y)=0, \quad \chi_e(x,y)=\overline{F}\lambda^{-1}\phi(x,y), \tag{15}$$

where the function $\phi(x,y)$ depends neither on the force $\overline{F}$ nor on the dimensionless thickness λ. Above a buckling threshold for the compressing forces, the flat solution Eq. (15) becomes unstable to small perturbations. Another buckled solution exists and may have a different dependence on the force $\overline{F}$. This does not affect the linear-response analysis, however, since the flat solution is unique for small $\overline{F}$.

We proceed with the boundary-layer analysis following Ref. [16]. This involves rescaling all variables by a power of λ,

$$\tilde{f}_i=\lambda^{\beta}f_i, \quad \tilde{\chi}_i=\lambda^{\delta}\chi_i, \quad \tilde{x}=\lambda^{0}x, \quad \tilde{y}=\lambda^{\beta}y, \tag{16}$$

with $\delta=2/3$ and $\beta=-1/3$ chosen in such a way as to balance the powers of λ in front of the terms in the Eqs. (14) that are relevant in the boundary layer. As in Ref. [16], we seek the solution to the rescaled equations as a series expansion in $\lambda^{2/3}$,

$$\tilde{f}_i=f_i^{(0)}+\lambda^{2/3}f_i^{(1)}+\lambda^{4/3}f_i^{(2)}+\cdots, \tag{17a}$$

$$\tilde{\chi}_i=\chi_i^{(0)}+\lambda^{2/3}\chi_i^{(1)}+\lambda^{4/3}\chi_i^{(2)}+\cdots. \tag{17b}$$

The equations for the zeroth order terms $f_i^{(0)}$ and $\chi_i^{(0)}$ read

$$\frac{\partial^4 f_i^{(0)}}{\partial\tilde{y}^4}=[\chi_i^{(0)},f_i^{(0)}]+\lambda^{1/3}\overline{F}[f_i^{(0)},\phi], \tag{18a}$$

$$\frac{\partial\chi_i^{(0)}}{\partial\tilde{y}^4}=-\frac{1}{2}[f_i^{(0)},f_i^{(0)}]. \tag{18b}$$

Let us examine the source term in detail,

$$[f_i^{(0)},\phi]=\frac{\partial^2 f_i^{(0)}}{\partial\tilde{x}^2}\frac{\partial^2\phi(\tilde{x},y)}{\partial y^2}+\lambda^{-2/3}\frac{\partial^2 f_i^{(0)}}{\partial\tilde{y}^2}\frac{\partial^2\phi(\tilde{x},y)}{\partial\tilde{x}^2}$$
$$-2\lambda^{-1/3}\frac{\partial^2 f_i^{(0)}}{\partial\tilde{x}\partial\tilde{y}}\frac{\partial^2\phi(\tilde{x},y)}{\partial\tilde{x}\partial y}. \tag{19}$$

The derivatives of ϕ are evaluated at $x=\tilde{x}$ and $y=\lambda^{1/3}\tilde{y}$. Since the rescaled variables are finite in the $\lambda\to 0$ limit, ϕ's behavior near $y=0$ determines the leading-order behavior of its derivatives in Eq. (19) in the $\lambda\to 0$ limit. The magnitude of the perturbation term is thus governed by $\tilde{F}=\lambda^{\rho}F$, where the value of the exponent ρ is determined by the behavior of the derivatives of ϕ near the ridge. For example, suppose all derivatives of ϕ are finite at $y=0$. This is indeed the case for the compression of a strip by a pair of point forces [21]. Then, the second term in Eq. (19) dominates so that $\rho=-1/3$. This behavior need not be generic since the derivatives of ϕ may vanish at $y=0$ by reasons of symmetry. Then the second term in Eq. (19) may vanish so that a higher-order term in λ dominates. This results in more positive value of ρ.

The solution $f_i^{(0)}$ and $\chi_i^{(0)}$ to Eqs. (18) can be sought as a series expansion in the small parameter $\tilde{F}$. Thus the zeroth-order term in the $\lambda^{2/3}$ expansion of the solution to the von Kármán equations in the presence of the external forces acting on the ridge is given by (up to quadratic terms in $\tilde{F}$)

$$f^{(0)}=f_i^{(0)}+f_e\simeq\lambda^{1/3}(f_0+\tilde{F}f_1+\tilde{F}^2f_2), \tag{20a}$$

$$\chi^{(0)}=\chi_i^{(0)}+\chi_e\simeq\lambda^{-2/3}(\chi_0+\tilde{F}\chi_1+\tilde{F}^2\chi_2)+\lambda^{-1}\overline{F}\phi. \tag{20b}$$

The terms linear in $\tilde{F}$ completely characterize the linear response of the ridge to this particular type of loading. In general, according to the postulated confinement property of the perturbing energy, second derivatives of f_1 and χ_1 possess the same qualitative features as those of f_0 and χ_0. In particular, the dominant second derivatives of f_1 and χ_1 are significant in the ridge region of characteristic width $\lambda^{1/3}$.

Substituting the $\widetilde{F}$ expansions into Eqs. (5), we obtain the expressions for the bending and stretching energies accurate up to terms of order $\overline{F^2}$,

$$E_{\text{bend}} \simeq E_0^b + E_1^b \overline{F} + E_2^b \overline{F^2}, \tag{21a}$$

$$E_{\text{str}} \simeq E_0^s + E_1^s \overline{F} + E_2^s \overline{F^2}. \tag{21b}$$

The energy of the unperturbed ridge as in Ref. [16] is $E_0^b \sim E_0^s \sim \lambda^{-1/3}$. Other E_i's are sums of integrals that involve second derivatives of f_i, χ_i, and ϕ. For example,

$$\begin{aligned} E_2^s \overline{F^2} &\simeq \lambda^2 \int d\overline{x}\, d\overline{y} (\lambda^{-2/3} \widetilde{F} \nabla^2 \chi_1 + \lambda^{-1} \overline{F} \nabla^2 \phi)^2 \\ &= \overline{F^2} \int d\overline{x}\, d\widetilde{y} \left[\lambda^{-1/3+2\rho} \left(\frac{\partial^2 \chi_1}{\partial \widetilde{y}^2} \right)^2 + \lambda^{\rho} \left(\frac{\partial^2 \chi_1}{\partial \widetilde{y}^2} \right) \nabla^2 \phi \right] \\ &\quad + \overline{F^2} \int d\overline{x}\, d\overline{y} (\nabla^2 \phi)^2. \end{aligned} \tag{22}$$

We must remark that the terms quadratic in $\overline{F}$ that involve f_2 and χ_2 cancel each other so that the linear in F correction to the potentials f and χ determines the quadratic correction to the total energy. This situation is common to all linear-response problems.

The leading-order behavior of E_1 and E_2 in the small thickness limit can be found by assuming, as before, that the corrections to the ridge solution f_1 and χ_1 are confined to the ridge region. The domain of integration in $\overline{y}$ in the integrals involving these ridge corrections as in Eq. (22) is thus of order $\lambda^{1/3}$. We can therefore obtain the asymptotic scaling of the coefficients in Eqs. (21). The bending and the stretching pieces scale with λ in the same way. The correction to the total energy is $E_2 \overline{F^2}$

$$E_1^{(b,s)} \sim A_1^{(b,s)} \lambda^{-1/3+\rho} + B_1^{(b,s)}, \tag{23a}$$

$$E_2 = E_2^s + E_2^b \sim A_2 \lambda^{-1/3+2\rho} + B_2 \lambda^{\rho} + C_2, \tag{23b}$$

where A_1^s, etc., are arbitrary coefficients that do not depend on λ in the $\lambda \to 0$ limit. If external stresses and curvatures given by the derivatives of χ_e and f_e, respectively, are zero on the ridge line and do not increase sufficiently rapidly away from the ridge, the exponent ρ will be positive and large so that the energy correction will be dominated by the last terms in the expressions for E_1 and E_2. These terms are identical to the energy of a flat sheet acted on by the external forces. If $\rho < 1/6$, however, the energy change is dominated in the small-thickness limit by the interaction of the ridge with the external forces given by the corrections to the ridge solution f_1, χ_1.

Equation (23) predict that both kinds of energy separately depend linearly on F. We demonstrate numerically in Sec. VII that upon application of point forces at the ridge vertices, each energy correction does indeed depend linearly on the applied force with the coefficient that scales with λ as predicted. The total energy can depend only on the square of the applied force since the boundary stresses and torques vanish for the undisturbed ridge so that the work done by the external force is exactly the change in the ridge's elastic energy. This means that the linear terms in $\overline{F}$ in the expressions (23) for E_{bend} and E_{str} must cancel each other, i.e., $E_1^s = -E_1^b$ to all orders in the $\lambda^{2/3}$ expansion ($A_1^s = -A_1^b$, $B_1^s = -B_1^b$, etc.). The numerics reported in Sec. VII convincingly show that it is indeed the case. The λ scaling of the ridge's elastic constant E_2 given in Eq. (23b) has also been shown to be consistent with the numerics.

When external forces distort the ridge, additional longitudinal strain results. We first define a ''vertex-to-vertex'' strain γ_v as the amount by which the vertices move closer together divided by X. We compare this quantity with the additional strain in the sheet that is the change in $\gamma_{xx} \simeq (1/Y) \partial^2 \chi / \partial y^2$. It can be found from the first order in $\widetilde{F}$ correction to χ Eq. (20). We can infer γ_v by inspection of the energy-force relation, since the work done by F is the change of the energy $E_2 \overline{F^2}$,

$$\gamma_v \sim \lambda E_2 \overline{F} \sim (A_2 \lambda^{2/3+2\rho} + B_2 \lambda^{1+\rho} + C_2 \lambda) \overline{F} \equiv G_{\text{ridge}}^{-1} \overline{F}, \tag{24}$$

whereas from Eq. (20) we obtain the change in the longitudinal strain in the sheet

$$\gamma_{xx}^{\text{add}} \sim \lambda^{2/3+\rho} \overline{F}. \tag{25}$$

Equation (25) gives another way to estimate the exponent ρ numerically.

This way of looking at the problem motivates the following consistency check of the perturbing energy confinement. An additional way of determining the λ scaling of the total-energy correction via $E_2 \overline{F^2} \sim G (\gamma_{xx}^{\text{add}})^2 w X / \kappa \sim \lambda^{-2/3+2\rho} \overline{w}$ must reproduce the scaling of E_2 obtained by explicit integration as in Eq. (23). Here $\overline{w} = w/X$ is the characteristic width of the region in which the perturbing energy is confined. Calculated by this method, the width $\overline{w} \sim \lambda^{1/3}$ is independent of the exponent ρ and scales with λ in the same way as the ridge width.

C. Buckling threshold

An important property of the ridge solution that is inaccessible by this simple perturbation scheme is the force required to *buckle* the ridge. In principle, one must solve Eqs. (18) and then perform a linear stability analysis of the solution to determine when the ridge will buckle. This task is intractable analytically due to the complexity of the equations. The asymptotic scaling of the buckling threshold may, nevertheless, be anticipated using the following argument. The undisturbed ridge solution f_0 and χ_0 is linearly stable against shape perturbations. Therefore, changes in this solution that destroy stability are likely to be of the order of the solution itself. To induce such changes, the additional terms in Eqs. (18) for the loaded ridge must be comparable in magnitude to the rest of the terms in the equations. Hence the parameter $\widetilde{F}$ that controls the magnitude of the additional terms in Eqs. (18) has to be of order unity $\widetilde{F} \sim 1$. This means that in the case of ridge compressed by vertex forces, the buckling threshold force scales as

$$\overline{F_{\text{crit}}} \sim \lambda^{-\rho}. \tag{26}$$

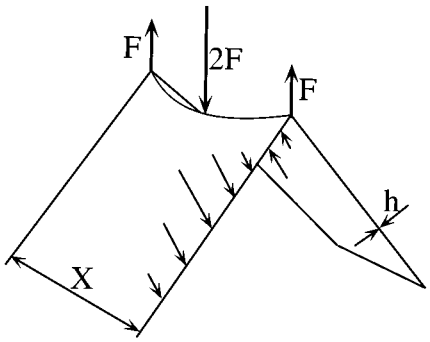

FIG. 3. Same strip bent by normal forces applied at the vertices as well as the middle of the ridge.

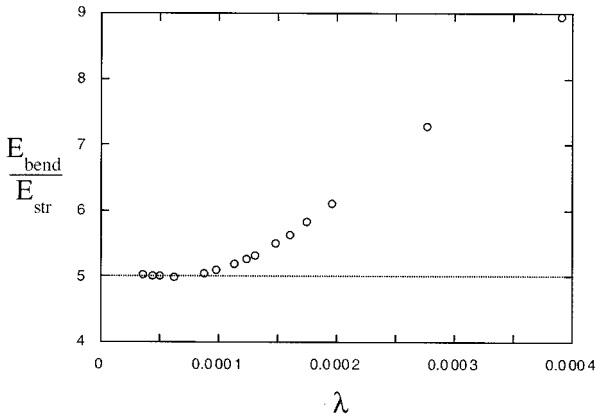

FIG. 4. Ratio of the total bending to the total stretching energy vs the dimensionless thickness λ for a regular tetrahedron of edge length $100b$. The asymptotic limit of 5 is approached for $\lambda \simeq 10^{-4}$.

This argument has a serious flaw. The scaling of the flat problem solution f_e and χ_e may be different for large forces F since additional solutions to the ''flat-problem'' may appear. This may result in a different value of the exponent ρ and thus a different scaling of the buckling threshold. The conjectured scaling of the critical load has two important implications. First, the additional longitudinal sheet strain at the buckling threshold given by the Eq. (25) is of order of the strain that existed in the ridge prior to compression. Second, the ridge energy correction at the buckling threshold value of the external force has the same asymptotic thickness scaling as the energy in the undisturbed ridge. This conclusion is supported numerically in Sec. VII. A corollary of this statement is that the applied load on a ridge does not have a decisive effect on its energy. The ridge buckles when its energy changes by a finite fraction. We will see in the following subsection that this argument applies to other types of loading as well. Therefore, any two unbuckled ridges in a crumpled sheet with comparable lengths and dihedral angles should have comparable energies, even though they have different loads.

D. Other types of loading

To describe elastic properties of the ridge in a way that is relevant to determination of the structure of the crumpled sheet we must investigate other types of loading. We first consider other loads that can be treated with the perturbation scheme developed above. These include normal forces acting on the minimal ridge. Having done that, we anticipate that in a crumpled sheet the assumptions that lead to the scaling laws for the energy corrections are violated.

Let us first use the perturbation scheme developed above to discuss other loads. The goal is to determine the weakest modulus of the ridge alluded to above. The perturbation treatment of this section relates the linear response of the flat sheet to the linear response of the ridge. We therefore anticipate that any perturbation that causes a large response in a flat sheet will also be relevant to the determination of the weakest ridge modulus. Since the bending rigidity $\kappa \sim Yh^3$ of an elastic sheet vanishes faster in the $h \to 0$ limit than the stretching modulus $G \sim Yh$, any perturbation that causes the sheet to bend will create a large response. We therefore consider normal forces on a ridge presented on Fig. 3.

Let us first describe the effect of these forces on a flat sheet. The scaling of the curvature potential f_e with force F can be found by noting that the torque of the external force is balanced by the flexural moment of the sheet due to its curvature $\kappa X \partial^2 f_e / \partial x^2 \sim FX$. Therefore, $f_e = \lambda^{-1} F \varphi$ is controlled by a single dimensionless parameter $\lambda^{-1} F$. Since the sheet is bent in the short direction, we can use the arguments of Sec. IV to show that this curvature persists up to a distance of order $L \sim X \lambda^{-1/3}$. The treatment of Sec. IV also determines the stresses in the strip. The dominant component of the stress is $\sigma_{yy} \sim Yh(a/L)^2$, where $a \sim f_e \sim X \lambda^{-1} F$. Hence the stress is of second order in the applied force F. The modified von Kármán equations (14) will thus have a first order in F source term due to f_e and a second order in F source term due to χ_e. One can now repeat the steps that lead from the modified von Kármán equations (14) via a rescaling transformation Eq. (16) to the perturbation expansion Eqs. (21). The only difference is the form of the flat solution f_e and χ_e.

With knowledge of the small-y behavior of the function φ, one can determine the exponent ρ that controls the ridge stiffness under this particular type of loading. The important second derivative $\partial^2 \varphi / \partial x^2$ is finite at the ridge. Therefore, $\rho = -4/3$. This means first that the linear response of the ridge to normal forces is qualitatively greater than to in-plane forces. Second, the normal force required to buckle the ridge $F_{\text{crit}} \sim \lambda^{4/3}$ is much smaller than in the case of longitudinal compression. The conjecture that the ridge buckles when its energy changes by a finite fraction can be made on the same basis as for the case of the longitudinal compression of the ridge.

We have thus shown that, depending on the symmetry of the applied load, the linear response of the ridge can vary considerably. It is unknown to us at this point whether the resistance of a crumpled sheet to further compression is determined solely by the weakest ridge modulus. It is certainly not inconceivable to imagine a situation in which a number of ridges in a crumpled sheet that form a kind of a ''structural skeleton'' are loaded in such a way that their linear response is given by a stronger modulus.

Let us finally discuss the applicability of the perturbation scheme developed here to ridges in a crumpled sheet. We anticipate the boundary stresses for the ridge in a crumpled

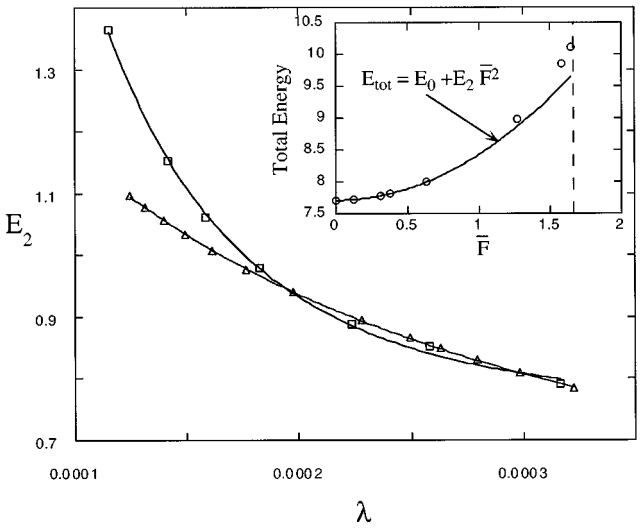

FIG. 5. Thickness dependence of the dimensionless coefficient E_2 in $E/\kappa \sim E_0 + E_2 \overline{F}^2$ for the strip of dimensions $43b \times 100b$ (squares) and tetrahedron of edge length $50b$ (triangles). The solid lines are fits according to Eq. (23) with $\rho = -1/3$ for the strip and $\rho = 0$ for the tetrahedron. Inset: plot of the total energy of a strip (in units of the bending rigidity κ) as a function of the applied force $\overline{F}$. The solid line is the quadratic fit to the first five points. Dashed vertical line marks the buckling threshold.

sheet to change by an amount proportional to a load. We cannot, therefore, utilize the perturbation method, developed in this section, to determine the scaling of the energy correction and the buckling threshold. Certain features of the conclusions that emerged from the perturbation analysis are likely to persist, however. We anticipate that the perturbing energy is confined to the ridge region. In addition, the change in the ridge longitudinal strain (the dominant ridge strain) must be proportional to the movement of the sheet caused by the external forces. The vertex-to-vertex strain is an example of such movement. The coefficient of proportionality is likely to scale as a power of the thickness λ. In most situations, one can make a reasonable guess to what

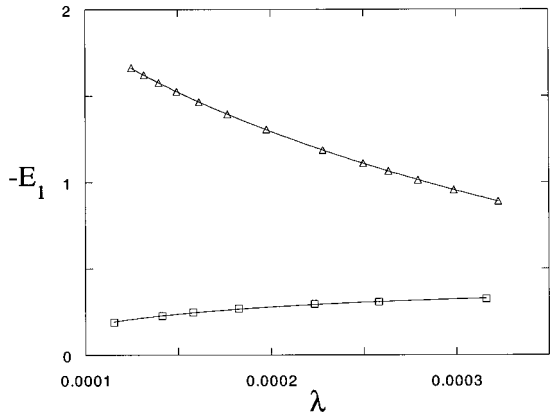

FIG. 6. Coefficient E_1^b of the linear dependence of the total bending energy in units of κ on the force $\overline{F}$ for the $43b \times 100b$ strip (squares) and the tetrahedron of size $50b$ (triangles). The solid lines are again fits according to Eq. (23) with the same values of the exponent ρ as in Fig. 5.

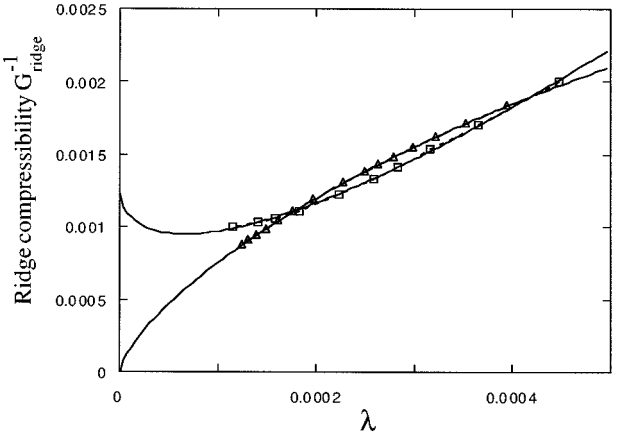

FIG. 7. Dimensionless coefficient G_{ridge}^{-1} of the linear $\overline{F}$ dependence of the ''vertex-to-vertex'' strain created by the external compressive force $\overline{F}$ for the strip (squares) and the tetrahedron (triangles). Solid lines are fits according Eq. (24). The tetrahedron ridge stiffness G_{ridge} is qualitatively greater in the limit of the vanishing thickness.

that power is. For example, the numerics reported in Sec. VII show that when a tetrahedron is compressed by point forces applied to its vertices, the additional ridge strain scales in the same way with λ as the vertex-to-vertex strain. This assumption, together with the notion of the perturbing energy confinement, is sufficient to determine the scaling of the energy correction.

VI. RIDGE INTERACTION

Ridges in a crumpled elastic sheet can interact in two distinct ways. First, distant parts of the sheet can press against a ridge. This type of interaction can be discussed using the framework developed in Sec. V. However, a quantitative understanding of the distribution of forces through the crumpled sheet is needed. Second, nearest-neighbor ridges can influence one another through the strains and curvatures they create in the sheet. We will concentrate on this particular aspect of the ridge interaction since we are able to obtain quantitative conclusions.

Two length scales characterize a ridge. Most of the ridge's elastic energy is confined within a strip of width $w \sim X\lambda^{1/3}$ around the ridge. Small curvatures and strains persist up to a distance $L \sim X\lambda^{-1/3}$ from the ridge. In a crumpled elastic sheet typical distances between ridges D are of the order of their length: $D \sim X$. Assuming that all ridges have the same characteristic size X, we are led to a conclusion that $w \ll D \ll L$ for most ridges. Therefore, the small residual strains and curvatures of a ridge will influence its neighbors in a way that is calculable within the framework of Sec. V. In fact, in Sec. IV we argued that there is a small transverse strain $\gamma_{yy} \sim a^2/L^2 \sim \lambda^{4/3}$ present in the sheet. This strain can be thought of as resulting from an external force $\overline{F} \sim \lambda^{1/3}$ that is stretching the sheet in the direction transverse to the ridge. Therefore, the stress potential function ϕ has a finite derivative $\partial^2\phi/\partial x^2$ at the ridge. According to the prescription of Sec. V, $\rho = -1/3$, so that the energy correction scales as

$$\delta E \sim \kappa\lambda^{-1/3+2\rho}\overline{F^2} \sim \kappa\lambda^{-1/3}. \tag{27}$$

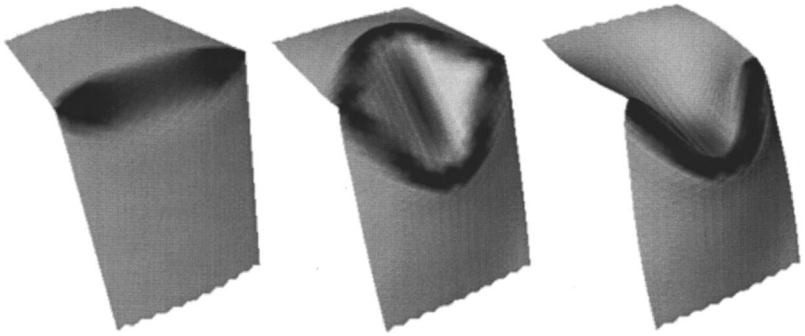

FIG. 8. Roof-shaped strip (left) collapsed by corner forces to obtain two stable buckled shapes as viewed obliquely from above. The value of the vertex forces must be reduced below the buckling threshold in order to achieve stability. Shading is proportional to the stretching energy density.

Note that the energy correction scales the same way with λ as the ridge energy. This means that even though the ridge wings carry a negligible amount of energy, they cause the total energy of the system to be changed by a finite fraction. This is not surprising since the transverse echo stresses discussed in Sec. IV are of the same magnitude as the transverse stresses in the ridge. The interaction energy of ridges in a strip geometry is studied numerically in the following section. It is found to be a few percent of the ridge energy in the small-thickness limit.

VII. NUMERICAL SIMULATION OF THE RIDGE PROPERTIES

In this section we use a lattice model of an elastic sheet of Ref. [20]. This model was used by the authors and others to verify a number of the ridge scaling properties [15,16]. The sheet is modeled by a triangular lattice of springs of equilibrium length b and spring constant K. A bending energy $J(1-\hat{\mathbf{n}}_1\cdot\hat{\mathbf{n}}_2)$ is assigned to each pair of adjacent lattice triangles with normals $\hat{\mathbf{n}}_1$ and $\hat{\mathbf{n}}_2$. When the strains are small compared to unity and radii of curvature are large compared to the lattice spacing b, this model bends and stretches like an elastic sheet of thickness $h=b\sqrt{8J/K}$ and bending modulus $\kappa=J\sqrt{3}/2$. We chose a discrete model of this sort over a conventional finite element scheme because the implementation of disclinations and boundary conditions is somewhat more straightforward in the lattice model. As a tradeoff, we must strictly control the finite-size lattice effect. Reference [16] makes a careful study of the lattice effects.

Ridges can be created either by imposing appropriate boundary conditions to a long strip of the simulated material or by introducing disclinations. We studied both types of shapes. First, we applied forces to the particles located on the long boundaries of a strip so as to constrain them to lie in different planes on each side of the ridge. The angle between the normals to these planes is 2α. Second, we connected a triangular piece of this simulated material into a regular tetrahedron so that each edge then became a ridge. A sequence of minimum energy shapes of different dimensionless thickness λ were obtained with the use of a conjugate gradient routine. External forces were then applied to the ridge vertices and the linear response to compression was measured as well as the buckling characteristics.

We first tested the virial theorem that predicts that if all of the elastic energy is concentrated in the ridges then the total bending energy is five times the total bending energy. In Fig. 4 we plot the ratio of the total bending to total stretching energies for the tetrahedron with edge length of $100b$. This ratio approaches the predicted value of $E_{\mathrm{bend}}/E_{\mathrm{str}}=5$ within a few percent for the values of dimensionless thickness $\lambda\leqslant 10^{-4}$. For the smallest values of λ on the plot the ratio deviates from the asymptotic value due to lattice effects. Thus the virial theorem is obeyed within our measurement precision.

The predictions of the scaling behavior of the ridge under external loading were done using a $43.3b\times 100b$ strip bent by boundary forces as well as a tetrahedron with an edge length of $50b$. We applied point forces to the vertex particles in either case in such a way as to compress the ridge. We first compressed a flat sheet to verify that stresses are finite on the line $y=0$. Then, the prediction for the exponent ρ defined in Sec. V is $\rho=-1/3$. The correction to the total elastic energy was found to depend on $\overline{F^2}$ as anticipated. The coefficient E_2 of $\overline{F^2}$ should scale with λ according to Eq. (23). Figure 5 is a plot of E_2 as extracted by a quadratic fit of the correction of the total elastic energy per ridge for the tetrahedron (triangles) and the strip (squares) as a function of λ. The inset of Fig. 5 shows the fit to the quadratic dependence of the total energy on the applied force.

The numerically accessible range of λ does not allow for a direct determination of the exponent ρ from the data. However, the strip data are consistent with the prediction for $\rho=-1/3$. However, the tetrahedron data are consistent with $\rho=0$ and inconsistent with $\rho=-1/3$ when fitted with the scaling form Eqs. (23) and (24). A given load appears to store qualitatively less energy for the tetrahedron than for the strip, i.e., the tetrahedron is qualitatively stiffer. This difference might be explained by noticing that in the case of the strip, the boundary shape B_0, which maintained the ridge, was fixed under the loading, whereas the effective boundary shape for the ridges in a tetrahedron changes when forces are applied. In addition, tangential stresses act on the the effective ridge boundary in a tetrahedron, whereas only normal boundary forces are present in the strip geometry. Therefore, the decomposition method of Sec. V cannot be used for the tetrahedron. The scaling of the tetrahedron stiffness implies that the additional strain due to the action of the compressive force is confined to the ridge region and scales the same way with the thickness λ as the vertex-to-vertex strain. These results are different from the situation in the strip. There, the vertex-to-vertex strain may be relaxed through bending so that the additional strain in the sheet is qualitatively weaker than the movement of the vertices would dictate if such relaxation were not possible.

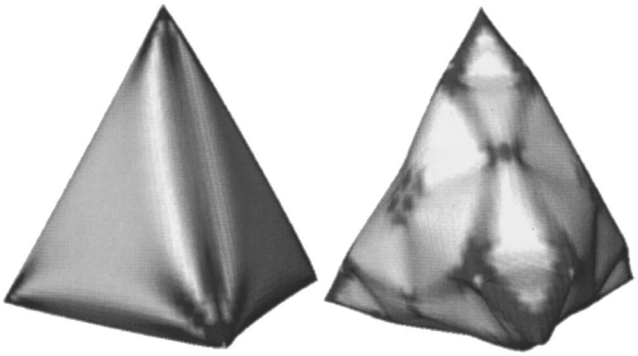

FIG. 9. Tetrahedron lattice (left) collapsed by application of vertex forces (right). A complicated buckling pattern results.

In Fig. 6 we plot E_1^b for both shapes extracted by a linear fit of the total bending energy as a function of F. The data are consistent with the prediction Eq. (23) for the same values of the exponents ρ as obtained from the scaling of E_2. Finally, we graph the coefficient G_{ridge}^{-1} of the linear dependence of the induced vertex-to-vertex strain on the applied force in Fig. 7. The data are consistent with the prediction Eq. (24). For comparison let us consider a flat strip. Its dimensionless stiffness G^{-1} to compression diverges as λ^{-1}, whereas its stiffness to bending vanishes as λ.

An important question that needs to be settled numerically is the buckling threshold of the ridge. The vertex forces were increased until the shape underwent a radical change. This seems to imply that buckling is a first-order phenomenon. In other words, there are several stable shapes other than the ridge for a range of compressive forces below the buckling threshold. Figure 8 shows two such buckled bent strip shapes. A buckled tetrahedron shape shown in Fig. 9 exhibits a more complex buckling pattern. Shading is proportional to the stretching energy density.

In Fig. 10 we plot the ratio of the energy correction to the total elastic energy of the undisturbed ridge at the bifurcation point of the loaded tetrahedron. This ratio seems to be approaching a constant in the $\lambda \to 0$ limit, which would agree with the prediction that the energy of a ridge can only change

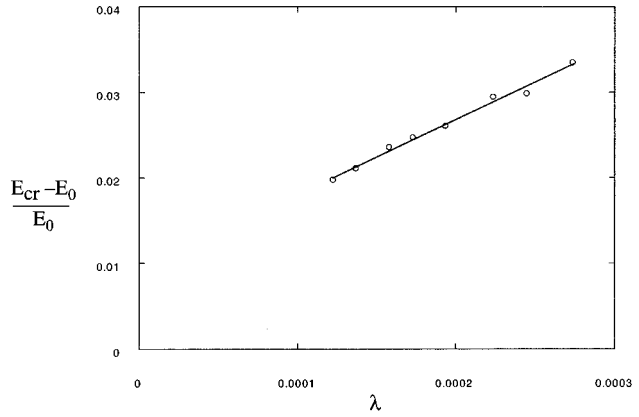

FIG. 10. Ratio of the energy correction at the buckling threshold of the tetrahedron of edge length $50b$ to the energy of the undisturbed tetrahedron as a function of the dimensionless thickness λ. The empirically drawn solid line suggests that the energy correction varies roughly linearly with λ.

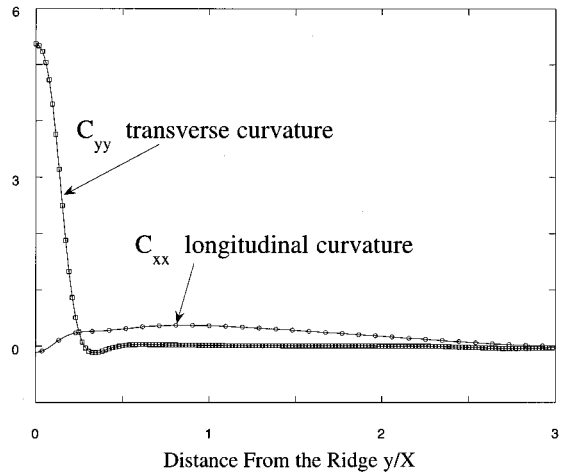

FIG. 11. Transverse ridge curvature C_{yy} (squares) and longitudinal curvature C_{xx} (circles) in units of X^{-1} along the perpendicular bisector of the ridge vs the distance from the ridge for a $52b \times 500b$ strip.

by a finite fraction before it buckles. More numerical tests are needed, however, to establish this assertion firmly. We did not attempt to characterize the buckling of the tetrahedron in further detail.

The large-distance behavior of the ridge wings was tested by using a long $52b \times 500b$ strip. Figure 11 displays the transverse curvature C_{yy} and the longitudinal curvature C_{xx} in units of X^{-1} along a perpendicular bisector of the ridge. A long, almost linear, decay of the C_{xx} is evident, whereas C_{yy} decays rapidly to zero. We extracted the decay length L for a sequence of ridges of varying λ and plotted the results in Fig. 12 versus the predicted scaling variable $\lambda^{-1/3}$. The linear fit shows that the data agree well with the prediction.

We next investigated the question of ridge interaction. Two parallel ridges were created in the strip geometry. We varied the distance between the ridges D as well as the thickness λ. Detailed interaction features that are shown in Fig. 13 for the $100b \times 130b$ strips for a fixed $\lambda = 0.0002$ depend

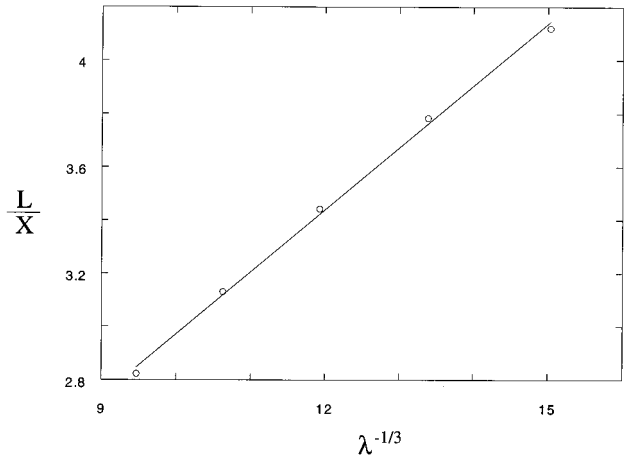

FIG. 12. Decay length of the longitudinal curvature L in the units of X vs the predicted scaling variable $\lambda^{-1/3}$ for a $52b \times 500b$ strip.

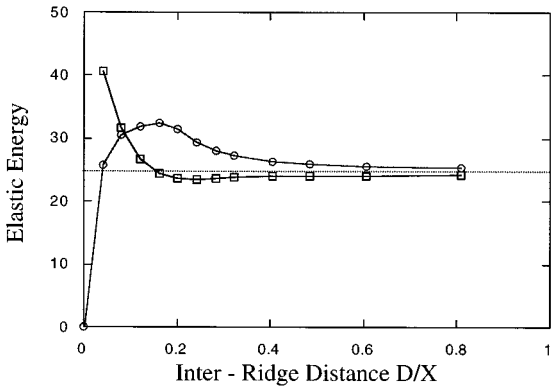

FIG. 13. Total elastic energy of a two-ridge configuration in the units of κ found from a $100b \times 130b$ strip bent in two places by 90° vs the distance between the ridges D. The thickness is $\lambda = 0.0002$. Squares correspond to the ridges that have the same orientation (configuration U), whereas the triangles correspond to two ridges of the opposite orientation (configuration Z).

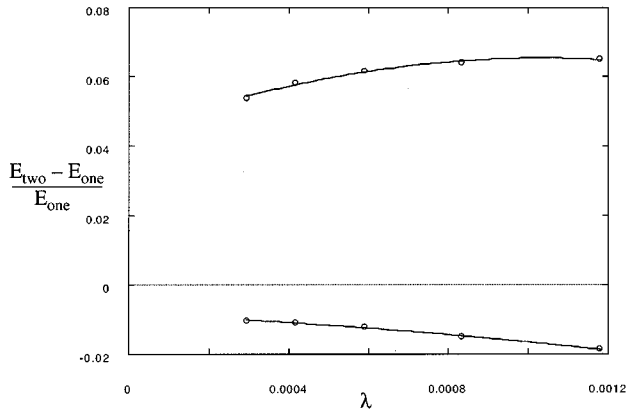

FIG. 14. Ratio of the difference of the total energy of two ridges and twice the energy of one ridge ΔE divided by the energy of one ridge E as a function of λ for a fixed interridge separation $D = 1.15X$. The data are obtained from simulation of a $52b \times 500b$ strip bent in two places. The lower curve corresponds to the configuration U in which the two ridges are have the same orientation and the upper curve corresponds to the ridges of the opposite orientation Z.

on the relative orientation of the ridges. If they are both concave (or both convex) as seen by looking down on the sheet from above (configuration U), they repel at short distances and attract at long distances. The situation is reversed if the ridges have different orientation (one is folded up and the other one down, or vice versa: configuration Z).

The signs of the interactions can be readily understood. At short distances, the two interacting ridges become a single ridge. If the two ridges have opposite signs, there is no ridge when they are brought together and thus the total energy is zero. If they have the same sign, the combined ridge has twice the dihedral angle α as the constituent ridge. Since ridge energy scales as $\alpha^{7/3}$ [16], the energy at $D = 0$ should be $2^{7/3}/2$ times that at $D = \infty$. The behavior of the interaction energy at large D is also understandable. Here the deformation between the ridges is minimal. For opposite sign ridges (configuration Z), the curvature fields created in the region between the ridges have opposite signs. For same-sign ridges shaped like ⊔, deformations caused by the two ridges at the midpoint reinforce each other. In a medium with a quadratic energy functional, such reinforcing deformations lead to a reduction in energy. Conversely, two opposite-sign ridges in a Z configuration have opposing deformations at the midpoint. This yields a repulsion.

For a complete account of the interaction energy, we must consider energy stored not only between the ridges, but within each ridge due to the presence of the other. To investigate such effects we made a long $52b \times 500b$ strip bent by 90° in two places. This creates two parallel ridges in the same strip whose relative orientation can be changed. In Fig. 14 we plot the difference of the elastic energy of the two ridges and twice the energy of one ridge ΔE divided by the energy of one ridge E as a function λ for a fixed interridge separation of $D = 1.15X$. The lower curve corresponds to the configuration in which the two ridges have the same orientation (U) and the upper curve corresponds to the ridges of the opposite orientation (Z). The results are consistent with the prediction that this ratio must approach a finite constant in the $\lambda \to 0$ limit. Therefore, the prediction that ridge interaction changes the system by a finite fraction is convincingly confirmed.

VIII. DISCUSSION

In this article we explored properties of the ridge singularity in thin elastic plates that may be relevant to a quantitative analysis of crumpled elastic membranes. A virial theorem that relates the bending and stretching contributions to the total elastic energy has been derived from an energy scaling argument and verified numerically. The virial theorem affords a useful test of elastic energy confinement. When most of the elastic energy is confined to the ridges the virial theorem predicts the ratio of the bending and stretching energies in the small-thickness limit.

We have developed a perturbation expansion scheme that allows one to calculate the effects of external forces on the scaling properties of the ridge singularity. We found that the problem can be decomposed into first solving for the effect of the external forces on the flat sheet χ_e and f_e and incorporating this solution into the equations that describe the ridge singularity in a way that is particularly convenient for a perturbation expansion. This method allows one to determine the scaling of the energy correction. This correction scales with the applied force squared and also a power of thickness that depends on the details of χ_e and f_e in the ridge region. Two different types of scaling were identified. Generally, an imposed strain comparable to the strain in a ridge stores an energy comparable to the ridge energy. This leads to an effective modulus of order $E_{\text{ridge}}/X^3 \sim Y\lambda^{8/3}$. A weaker modulus is possible for isolated ridges with stress-free boundaries since the imposed strain can be relaxed in ways not accessible to ridges in a crumpled sheet.

A feature common to all types of ridge loading is that the ridge solution becomes unstable when the external forces change the energy of the ridge by an amount that is comparable to the original undisturbed ridge energy. This discovery gives justification to a claim that the energy of a crumpled

elastic sheet can be found once the ridge network is characterized in terms of the ridge sizes X_i and their dihedral angles θ_i [16].

We have found that the large distance part of the ridge solution that matches onto the boundary-layer solution exhibits scaling with the thickness λ. We have established by an energy scaling argument as well as an extension of the scaling analysis of the von Kármán equations that small stresses and strains persist up to a distance $L \sim X\lambda^{-1/3}$ away from the ridge. Using the framework developed in this paper, we found that the main implication of the ridge wings is that ridges located at distances $D \ll L$ away from each other interact in a way that changes their total energy by a small but finite fraction.

In the future we plan to build a model for a quantitative characterization of the ridge network in crumpled sheets that incorporates the properties of ridges uncovered in this article and makes a prediction for the ridge size distribution. We hope to characterize the buckling behavior more thoroughly and verify our hypothesis that the generic scaling of the modulus is that of the tetrahedron studied here.

ACKNOWLEDGMENTS

The authors are grateful to E. M. Kramer for many productive and stimulating discussions. This work was supported in part by the MRSEC Program of the National Science Foundation under Grant No. DMR-9400379 and by the National Science Foundation Grant No. DMR-9528957.

[1] E. Sackmann, P. Eggl, C. Fahn, H. Bader, H. Ringsdorf, and M. Schollmeier, Ber. Bunsenges. Phys. Chem. **89**, 1198 (1985).

[2] M. S. Spector, E. Naranjo, and J. A. Zasadzinski, Phys. Rev. Lett. **73**, 2867 (1994).

[3] R. R. Chianelli, E. B. Prestrige, T. A. Pecoraro, and J. P. DeNeufville, Science **203**, 1105 (1979).

[4] P. Stutenkemper and R. Brasche, in *Occupant Protection in Frontal Impacts*, Proceedings of the Seventh International Technical Conference on Experimental Safety Vehicles, Paris, 1979 (U.S. Department of Transportation, Washington, D.C., 1980).

[5] R. E. Newton, in *Shock and Vibration Handbook*, edited by C. M. Harris and C. E. Crede (McGraw-Hill, New York 1988), p. 31-1; P. E. Franklin and M. T. Hatae, *ibid.* p. 41-1.

[6] *Post-Buckling of Elastic Structures*, Proceedings of the Euromech Colloquium, No. 200, Matrafured, Hungary, 1985, edited by J. Szabó (Elsevier, Amsterdam, 1986).

[7] E. H. Mansfield, *The Bending and Stretching of Plates* (Pergamon, New York, 1964).

[8] Y. C. Fung and W. H. Wittrick, Q. J. Mech. Appl. Math. **8**, 191 (1955).

[9] H. Reissner, *Spannugen in Kugelschalen-(Kuppeln)* (Festschrift Mueller-Breslau, Leipzig, 1912), p. 181.

[10] A. E. H. Love, *A Treatise on the Mathematical Theory of Elasticity*, 4th ed. (Cambridge University Press, Cambridge, 1927), pp. 29 and 459.

[11] D. G. Ashwell, Proc. Roy. Soc. London Ser. A **214**, 98 (1952).

[12] N. Yamaki, *Elastic Stability of Circular Cylindrical Shells* (North-Holland, New York, 1984).

[13] T. von Kármán and H. S. Tsien, J. Aerosol Sci. **8**, 303 (1941).

[14] R. Scheidl and H. Troger, Comput. Struct. **27**, 157 (1987).

[15] A. E. Lobkovsky *et al.*, Science **270**, 1482 (1995).

[16] A. E. Lobkovsky, Phys. Rev. E **53**, 3750 (1996).

[17] T. A. Witten and Hao Li, Europhys. Lett. **23**, 51 (1993).

[18] L. D. Landau and E. M. Lifshitz, *Theory of Elasticity* (Pergamon, Oxford, 1986), Chap. II. Our cylindrical modulus κ is denoted there as D.

[19] L. D. Landau and E. M. Lifshitz, *Mechanics*, 3rd ed. (Pergamon, Oxford, 1994).

[20] H. S. Seung and D. R. Nelson, Phys. Rev. A **38**, 1005 (1988).

[21] L. D. Landau and E. M. Lifshitz, *Theory of Elasticity* (Ref. [18]), Problem 1 to Sec. 12.